Enhanced near-field thermal radiation and reduced Casimir stiction between doped-Si gratings

Xianglei Liu, Bo Zhao, and Zhuomin M. Zhang*
George W. Woodruff School of Mechanical Engineering, Georgia Institute of Technology, Atlanta, Georgia 30332, USA
(Received 23 March 2015; published 25 June 2015)

Based on the scattering theory, simultaneously enhanced energy transport and suppressed momentum exchange are demonstrated by patterning doped-silicon surfaces in the near field. The radiative heat flux between doped-silicon gratings exceeds that between planar surfaces and can be one or even two orders of magnitude higher than what is predicted by the geometry-based Derjaguin proximity approximation (PA). The underlying mechanism is interpreted as due to the excitation of broadband hyperbolic modes that facilitate photon tunneling, especially when the period is small. This is confirmed by a comparison of the results from the scattering theory with those from the effective-medium theory. The Casimir force, which may cause stiction and even failure of mesoscopic devices, is reduced with the grating structures as predicted by both the scattering theory and PA. However, depending on the separation distance, the PA may over- or underpredict the Casimir force.

DOI: 10.1103/PhysRevA.91.062510 PACS number(s): 31.30.jh, 44.40.+a, 73.20.Mf, 03.70.+k

I. INTRODUCTION

Near-field thermal radiation and Casimir interaction induced by quantum mechanical electromagnetic fluctuations have received much attention in recent decades. Tunneling of evanescent waves enables near-field radiative heat flux between two close bodies to exceed the well-known Stefan-Boltzmann law, the upper limit for the far-field thermal radiation, especially when hyperbolic modes or surface modes such as surface plasmon polaritons (SPPs) and surface phonon polaritons are excited [1–7]. The promising applications of near-field heat transfer in thermophotovoltaics [8–14], thermal imaging [15,16], thermal modulators [17–23], and local thermal management [24,25] have motivated researchers to explore nanostructures capable of supporting higher efficiencies or larger heat fluxes than those between planar surfaces. Deep subwavelength metamaterials, such as nanowires [26–28], nanoholes [29–31], and carbon nanotubes [32–34], have recently been demonstrated to have better near-field heat transfer performance than bulk materials with planar surfaces. Most of these works are based on the effective-medium theory (EMT), which is valid only when the gap distance is much greater than the period of nanostructures [35]. Additionally, controlling the surface roughness of nanowires or nanotubes within submicron gap distances to avoid contact is very difficult. Binary gratings are another type of promising candidates for near-field radiation control and the grating structures with desired dimensions can be realized using micro- and nanofabrication technologies.

Although the EMT is questionable at gap distances comparable to or smaller than the period, small gap spacing is often desired for applications such as energy harvesting and effective heat removal. However, the near-field energy transport for small gap separations may approach the localized situation when the interactions are important only between nearby surfaces, as is the case described by the geometry-based Derjaguin proximity approximation (PA) [36,37]. The implication of such a localization phenomenon is that, in the near field, nanostructures may not achieve higher radiative heat flux than the bulk counterparts with the same gap distance, measured by the minimum separation between the two materials. Lussange *et al.* [38] investigated two corrugated silica plates considering various geometry parameters and found that the PA works well for aligned silica gratings. This is not surprising since the lateral propagation length of evanescent surface modes is short especially for high-k modes; subsequently, the heat transport tends to be localized. On the other hand, Guérout *et al.* [39] predicted that corrugating gold film can prominently improve the near-field heat transfer over bulk counterparts. The mechanism lies in the shifting of guided modes to the lower-frequency region with increasing corrugation depth, where the energy of Planck's oscillators is higher. Nevertheless, for noble metals, surface modes generally exist in the violet or ultraviolet region and can barely be thermally excited to enhance radiative energy transfer unless at extremely high temperatures. As a result, they are usually poor near-field emitters compared with those for which surface modes lie in the infrared region that can be easily thermally excited, such as silica and doped silicon. It has been noted that covering graphene will break the PA limit and help to achieve delocalized radiative heat transfer between corrugated silica surfaces due to the large propagation length of graphene plasmons [40]. One of the objectives of the present work is to investigate doped-silicon gratings using the scattering theory and to analyze various geometric parameters to see whether the PA limit will be valid and whether the EMT will be applicable under certain circumstances. It is hoped that large enhancement of near-field radiative transfer can be achieved with corrugated doped-silicon surfaces.

Another aspect of this study is the calculation of forces between doped-silicon gratings in close proximity. In practical applications of microelectromechanical systems (MEMS) and nanoelectromechanical systems for thermal management, the Casimir stiction between working parts has to be considered even in vacuum. The Casimir interaction, arising from momentum exchange between fluctuating electromagnetic waves, always accompanies near-field heat transfer and is mainly induced by quantum fluctuations along with thermal fluctuations [41–43]. The Casimir force can be as large as 130 kPa at a gap spacing of 10 nm and thus could cause a failure of mesoscopic systems and devices [44]. It is necessary to examine how nanostructures affect the Casimir force.

*Corresponding author: zhuomin.zhang@me.gatech.edu

This work investigates both the radiative energy transport and the Casimir interaction between doped-silicon gratings. Three formulations based on the scattering theory [38–40,45], EMT [18,31,46,47], and PA are employed for the calculation and analysis. The results are compared for various geometries to explore the potential for near-field heat-transfer enhancement using gratings. Because of the unique characteristics of doped silicon and doped-silicon nanostructures, the underlying mechanism for the near-field heat transfer is very different from guide modes in gold gratings or surface modes in graphene-covered nanostructures. The reason why PA fails to predict near-field radiative heat transfer between doped-silicon gratings is explored. In particular, broadband hyperbolic modes are identified by comparison of the energy transmission coefficients predicted by both the scattering theory and EMT. The effect of the lateral displacement between the gratings for the emitter and receiver is also discussed.

II. THEORETICAL FORMULATION

The schematic of near-field heat transfer and Casimir interaction between gratings separated by a vacuum gap of distance d is shown in Fig. 1, where P is the period, W is the grating width, and H is the grating thickness. Note that δ is the lateral displacement between the two gratings with identical geometry. In all the calculations, temperatures of the emitter and receiver are set to $T_1 = 310\,\mathrm{K}$ and $T_2 = 290\,\mathrm{K}$, respectively. Doped silicon is used as the base material for both the grating region (or film) and the substrate (bulk solid adjacent to the grating film) since it can support SPPs in the infrared region with good tunability [48–51]. The n-type doping concentration is chosen as $10^{20}\,\mathrm{cm}^{-3}$, at which the dielectric function can be described by a simple Drude model [48,52]: $\varepsilon_{D-\mathrm{Si}}(\omega) = 11.7 - \omega_\mathrm{p}^2/(\omega^2 + i\gamma\omega)$, where the plasma frequency $\omega_\mathrm{p} = 1.08 \times 10^{15}\,\mathrm{rad/s}$ and scattering rate $\gamma = 9.34 \times 10^{13}\,\mathrm{rad/s}$ are evaluated at the average temperature of the two gratings, i.e., 300 K.

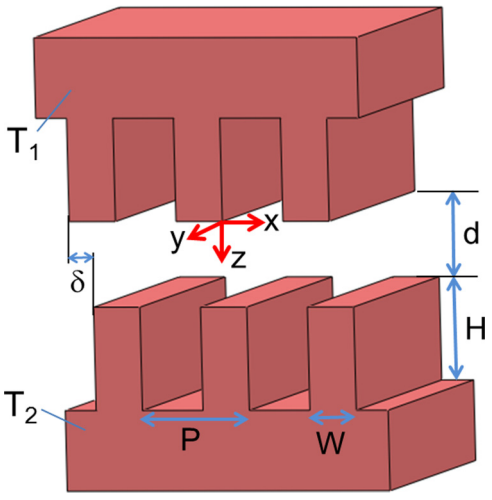

FIG. 1. (Color online) Schematic of near-field radiative heat transfer between two one-dimensional doped-silicon gratings with a lateral displacement of δ. For both gratings, the height, period, and width are H, P, and W, respectively. The temperatures of the two gratings are set as $T_1 = 310\,\mathrm{K}$ and $T_2 = 290\,\mathrm{K}$, respectively, for all calculations.

A. Exact solutions based on scattering theory

The near-field radiative heat transfer between two gratings based on the scattering theory is presented by [38,39]

$$Q = \frac{1}{8\pi^3}\int_0^\infty [\Theta(\omega,T_1) - \Theta(\omega,T_2)]\,d\omega \times \int_{-\pi/P}^{\pi/P}\int_{-\infty}^{\infty} \xi(\omega,k_x,k_y)\,dk_x dk_y, \tag{1}$$

where $\Theta(\omega,T) = \hbar\omega/e^{\hbar\omega/k_\mathrm{B}T} - 1$ is the average energy of Planck's oscillator and $\xi(\omega,k_x,k_y)$ is the energy transmission coefficient that depends on the frequency and wave vector components k_x and k_y considering all the polarization states. Based on the scattering theory, the energy transmission coefficient is given as [38,39]

$$\xi(\omega,k_x,k_y) = \mathrm{Tr}(\mathbf{D}\mathbf{W}_1\mathbf{D}^\dagger\mathbf{W}_2), \tag{2}$$

$$\mathbf{D} = (\mathbf{I} - \mathbf{S}_1\mathbf{S}_2)^{-1}, \tag{3}$$

$$\mathbf{W}_1 = \sum_{-1}^{\mathrm{pw}} -\mathbf{S}_1 \sum_{-1}^{\mathrm{pw}} \mathbf{S}_1^\dagger + \mathbf{S}_1 \sum_{-1}^{\mathrm{ew}} - \sum_{-1}^{\mathrm{ew}} \mathbf{S}_1^\dagger, \tag{4}$$

$$\mathbf{W}_2 = \sum_{1}^{\mathrm{pw}} -\mathbf{S}_2^\dagger \sum_{1}^{\mathrm{pw}} \mathbf{S}_2 + \mathbf{S}_2^\dagger \sum_{1}^{\mathrm{ew}} - \sum_{1}^{\mathrm{ew}} \mathbf{S}_2, \tag{5}$$

where $\mathbf{S}_1 = \mathbf{R}_1$, $\mathbf{S}_2 = e^{ik_{z0}d}\mathbf{R}_2 e^{ik_{z0}d}$, and the dagger denotes the Hermitian adjoint. Note that $\mathbf{R}_1$ or $\mathbf{R}_2$ is a $(4N+2)\times(4N+2)$ reflection matrix obtained by using rigorous coupled-wave analysis (RCWA) [53,54]. Here N is the highest diffraction order used in the computation and should be large enough to ensure convergence. Note that k_x is folded into the first Brillouin zone since the structure is periodic in the x direction. Operators $\sum_{-1\,(1)}^{\mathrm{pw\,(ew)}}$ identifying propagating and evanescent modes are presented in Ref. [38]. The accuracy of the numerical method is solely limited by the diffraction orders used in the RCWA. The calculation results are validated by comparison with previous works [38,39] and the convergence is tested using a sufficiently large number of diffraction orders. The numerical solutions obtained by the scattering theory are treated as exact results in this work for the purpose of comparison.

B. Effective-medium theory

Alternatively, when the gap distance is much larger than the period of nanostructures, the EMT combined with fluctuational electrodynamics can be adopted to predict the near-field heat flux. In this circumstance, the grating film can be homogenized as a uniaxial material with the optical axis lying in the x-y plane. The effective dielectric functions of the equivalent homogenized thin film for the grating region are given by [31]

$$\varepsilon_O = (1-f) + \varepsilon_{D\text{-Si}}\,f, \tag{6}$$

$$\varepsilon_E = \frac{\varepsilon_{D\text{-Si}}}{(1-f)\varepsilon_{D\text{-Si}} + f}, \tag{7}$$

where ε_O and ε_E are the dielectric functions for the electric field perpendicular and parallel to the optical axis, respectively, and $f = W/P$ is the filling ratio. For the configuration shown in Fig. 1, the optical axis is parallel to the x axis.

The radiative heat flux between thin grating films on doped-Si substrates based on the EMT can be expressed as [18,31]

$$Q = \frac{1}{8\pi^3}\int_0^\infty [\Theta(\omega,T_1) - \Theta(\omega,T_2)]d\omega \times \int_0^{2\pi}\int_0^\infty \xi(\omega,\beta,\phi)\beta d\beta d\phi, \tag{8}$$

where $\beta = \sqrt{k_x^2 + k_y^2}$ is the transverse wave vector, ϕ is the azimuthal angle, and $\xi(\omega,\beta,\phi)$ is the energy transmission coefficient considering polarization coupling and can be expressed as [31]

$$\xi(\omega,\beta,\phi) = \begin{cases} \mathrm{Tr}[(\mathbf{I} - \mathbf{R}_2^\dagger\mathbf{R}_2)\mathbf{D}(\mathbf{I} - \mathbf{R}_1\mathbf{R}_1^\dagger)\mathbf{D}^\dagger], & \beta < k_0 \\ \mathrm{Tr}[(\mathbf{R}_2^\dagger - \mathbf{R}_2)\mathbf{D}(\mathbf{R}_1 - \mathbf{R}_1^\dagger)\mathbf{D}^\dagger]e^{-2|k_{z0}|d}, & \beta > k_0, \end{cases} \tag{9}$$

where $\mathbf{D} = (\mathbf{I} - \mathbf{R}_1\mathbf{R}_2 e^{2ik_{z0}d})^{-1}$ is a Fabry-Pérot-type denominator representing the multiple reflections inside the vacuum cavity and $\mathbf{R}_1$ and $\mathbf{R}_2$ are the 2×2 reflection coefficient matrices including both the copolarization (r_{ss} and r_{pp}) and cross-polarization (r_{sp} and r_{ps}) components. Since the two gratings are parallel to each other, the optical axes are also parallel, making the calculations much easier. Note that ϕ defines the plane of incidence and the rotation of the plane of incidence is equivalent to the rotation of the optical axis of the anisotropic film. The dielectric function tensor of the film with respect to the plane of incidence is given as

$$\bar{\bar{\varepsilon}} = \begin{pmatrix} \varepsilon_O\cos^2\chi + \varepsilon_E\sin^2\chi & (\varepsilon_O - \varepsilon_E)\sin\chi\cos\chi & 0 \\ (\varepsilon_O - \varepsilon_E)\sin\chi\cos\chi & \varepsilon_O\sin^2\chi + \varepsilon_E\cos^2\chi & 0 \\ 0 & 0 & \varepsilon_O \end{pmatrix}, \tag{10}$$

where χ is the angle between the optical axis and the normal of the plane of incidence. In Ref. [31], expressions for the reflection coefficient matrix were given when the anisotropic medium is semi-infinite. These expressions are extended in the present study to treat the anisotropic film with thickness of H, i.e., the same as the grating height, on top of a bulk substrate.

C. Proximity approximation

The PA, which is based on pairwise addition, assumes near-field heat transfer between complex structures to be localized without considering interactions between neighboring unit cells. The resulting radiative heat flux can be calculated as a weighted average of plane-plane configurations at different gap distances. For one-dimensional gratings with $f \leqslant 0.5$, the radiative heat flux predicted by the PA can be written as

$$Q_{\mathrm{PA}} = \begin{cases} \frac{fP-\delta}{P}Q_d + \frac{2\delta}{P}Q_{d+H} + \frac{P-fP-\delta}{P}Q_{d+2H}, & \delta \leqslant fP \\ 2fQ_{d+H} + (1-2f)Q_{d+2H}, & fP < \delta \leqslant 0.5P. \end{cases} \tag{11}$$

Similarly, when $f > 0.5$, the PA gives

$$Q_{\mathrm{PA}} = \begin{cases} \frac{fP-\delta}{P}Q_d + \frac{2\delta}{P}Q_{d+H} + \frac{P-fP-\delta}{P}Q_{d+2H}, & \delta \leqslant (1-f)P \\ (2f-1)Q_d + 2(1-f)Q_{d+H}, & (1-f)P < \delta \leqslant 0.5P. \end{cases} \tag{12}$$

Here Q_d, Q_{d+H}, and Q_{d+2H} are the radiative heat flux for plane-plane configurations at gap distances of d, $d+H$, and $d+2H$, respectively. Due to symmetry, the range of lateral displacement that needs to be considered is from 0 to $P/2$ only. Note that Eqs. (11) and (12) can be used directly to calculate the Casimir interaction by replacing the radiative heat flux with the Casimir force.

D. Calculation of the Casimir force

The Casimir attraction between gratings at finite temperature T at equilibrium conditions can be obtained using the previously discussed scattering theory as [53,54]

$$F = 2\pi k_B T {\sum_{n=0}^{\infty}}' \int_{-\pi/P}^{\pi/P}\int_{-\infty}^{\infty} \mathrm{Tr}\left[(\mathbf{I} - \mathbf{M}_n)^{-1}\frac{\partial \mathbf{M}_n}{\partial d}\right]dk_x dk_y, \tag{13}$$

where the prime on the summation operator means that the $n = 0$ term should be taken with a factor of 0.5. Equation (13) is similar to Eq. (1) to some extent, but the summation here is exerted over the Matsubara imaginary frequencies $\zeta_n = i\omega_n = i2\pi nk_BT/\hbar$. Note that T is set to be 300 K, the average of T_1 and T_2, and the nonequilibrium effects are neglected given that the temperature difference between T_1 and T_2 is small (20 K) and the zero-point energy has the dominant contribution at submicron gap spacings around room temperature. The matrix $\mathbf{M}_n$ can be described by the reflection coefficients $\mathbf{R}_1$ and $\mathbf{R}_2$ at the Matsubara frequencies, obtained by using the RCWA [53].

III. RESULTS AND DISCUSSION

A. Enhancement of near-field heat flux

In this study, the following geometric parameters are chosen as the default values unless otherwise specified: $P = 200$ nm, $d = 400$ nm, $f = 0.2$, $H = 1\,\mu$m, and $\delta = 0$ (aligned case). The radiative heat flux between two gratings as a function of the filling ratio is plotted in Fig. 2(a), while other geometric parameters are set as the default values. When $f = 1$, both results reduce to the case for two planar substrates (bulk doped silicon) for which the near-field heat flux is 294 W/m^2. The radiative heat flux predicted by the PA decreases linearly as f is reduced, which is opposite to the trend calculated by the scattering theory (exact). When $f = 0.05$, the heat flux

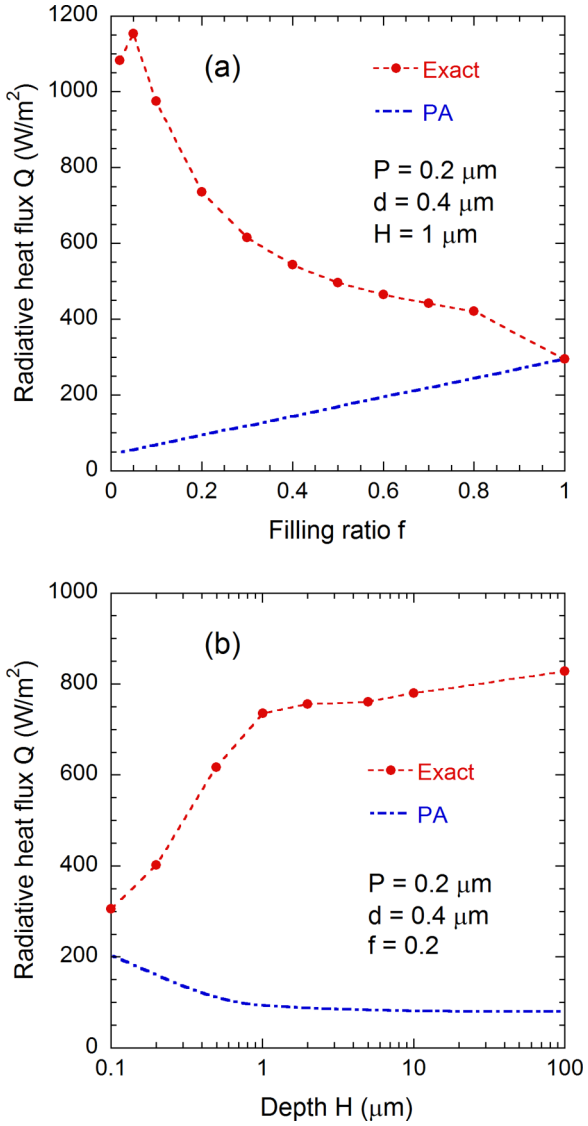

FIG. 2. (Color online) Radiative heat flux as a function of (a) filling ratio $f = W/P$ and (b) grating height H, calculated from both the scattering theory (indicated as exact) and the PA method for aligned gratings. Only one parameter is changed while the rest are fixed as the default values $P = 200\,\text{nm}$, $d = 400\,\text{nm}$, $f = 0.2$, and $H = 1\,\mu\text{m}$.

achieves a maximum value of 1154 W/m^2, which is 20.7 times larger than what is predicted by the PA, breaking down the assumption of localized radiative transport. Further decreasing f will result in a reduction of the heat flux. Of course $f = 0$ implies the situation between two planar media with a gap distance $d + 2H$ and both the exact solution and PA method give the same result. However, even though the filling ratio is as small as 0.01, the heat flux is enhanced to over 1000 W/m^2 as predicted by the scattering theory. The radiative heat transfer for doped-silicon gratings is very efficient with higher heat flux at any practical filling ratio than that for bulk doped silicon. This is in contrast to aligned gratings made of polar materials, such as silica, which have been demonstrated to support localized heat transport due to the short lateral propagation length of surface phonon modes [38]. For this reason, the PA works well for aligned silica gratings and as such silica nanostructures can barely outperform bulk materials in terms of near-field radiative heat transfer [38,40]. For doped-silicon gratings, reducing the filling ratio can result in an enhancement of more than two orders of magnitude over that predicted by the geometry-based PA.

As shown in Fig. 2(b), the near-field heat flux increases with the grating depth according to the exact solution, while the PA predicts the opposite trend. When H is close to zero, the calculated radiative heat flux based on the exact solution recovers the value of 294 W/m^2, i.e., between two planar substrates. The heat flux between gratings increases slowly and tends to saturate when the grating thickness exceeds 10 μm, suggesting that the radiation penetration depth of the grating film is on the order of several micrometers. When H is further increased, the substrates beyond the grating region contribute little to near-field radiative transfer.

B. Comparison of the exact solutions with the EMT and PA

The near-field radiative heat flux between gratings based on the scattering theory is compared with the predictions from the EMT and PA as shown in Fig. 3. In order to identify the region where doped-silicon gratings perform better than bulk counterparts, the radiative heat flux for bulk doped silicon is also shown in Fig. 3. The effect of period on the calculated heat flux is shown in Fig. 3(a), in which d, f, and H are kept at the default values of 400 nm, 0.2, and 1 μm, respectively. The predicted heat fluxes by the EMT and PA are independent of the period for aligned identical gratings and thus are flat lines. Interestingly, as the period decreases, the heat flux predicted by the scattering theory (exact) approaches and finally coincides with that by the EMT. For example, when $P = 20\,\text{nm}$ the heat flux from the exact solution is 941.54 W/m^2, which is essentially the same as the EMT prediction of 941.58 W/m^2. With decreasing period and the width of the gratings, it becomes difficult for waves to sense the small features and therefore homogenizing the grating as an effective medium becomes more reasonable. Similar observations were shown for metallodielectric metamaterials in Ref. [35], where quantitative criteria for the validity of EMT in predicting radiative heat transfer between multilayers are given.

On the other hand, if the period becomes large enough, the radiative heat transfer is expected to achieve the value predicted by the PA due to the negligible interactions between different unit cells nearby. At $P = 20\,\mu\text{m}$, the heat flux of 96.0 W/m^2 as predicted by the scattering theory is only slightly higher than the PA limit of 93.3 W/m^2. The exact solutions lie between the upper asymptotic line governed by the EMT limit and the lower asymptotic line governed by the PA limit. Corrugating bulk doped silicon helps to enhance the radiative heat flux for small periods, where the many-body interactions between neighboring unit cells become nontrivial.

The near-field radiative heat flux for gap distance varying from 10 nm to 10 μm is shown in Fig. 3(b) when other geometric parameters are fixed at the default values. The agreement between the scattering theory and EMT is excellent when $d > 0.6\,\mu\text{m}$. The reason is that the number of contributing modes decreases with increasing gap spacing [35,55]. Then,

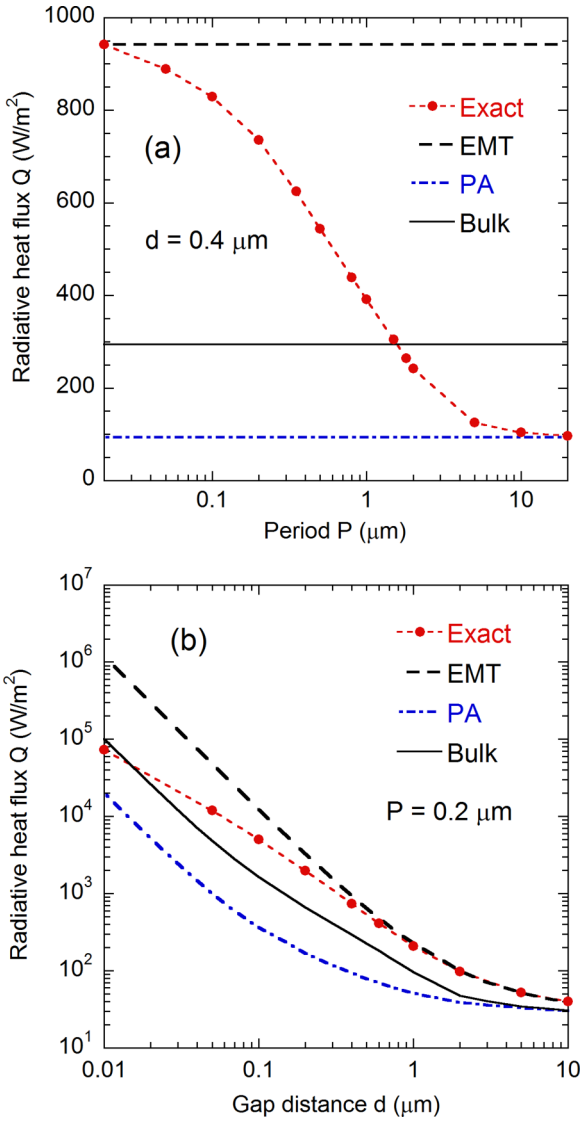

FIG. 3. (Color online) Comparison of heat flux calculated from the scattering theory with EMT, PA limit, and bulks. (a) Effects of period for $d = 0.4\,\mu$m and (b) effects of gap distance at $P = 0.2\,\mu$m.

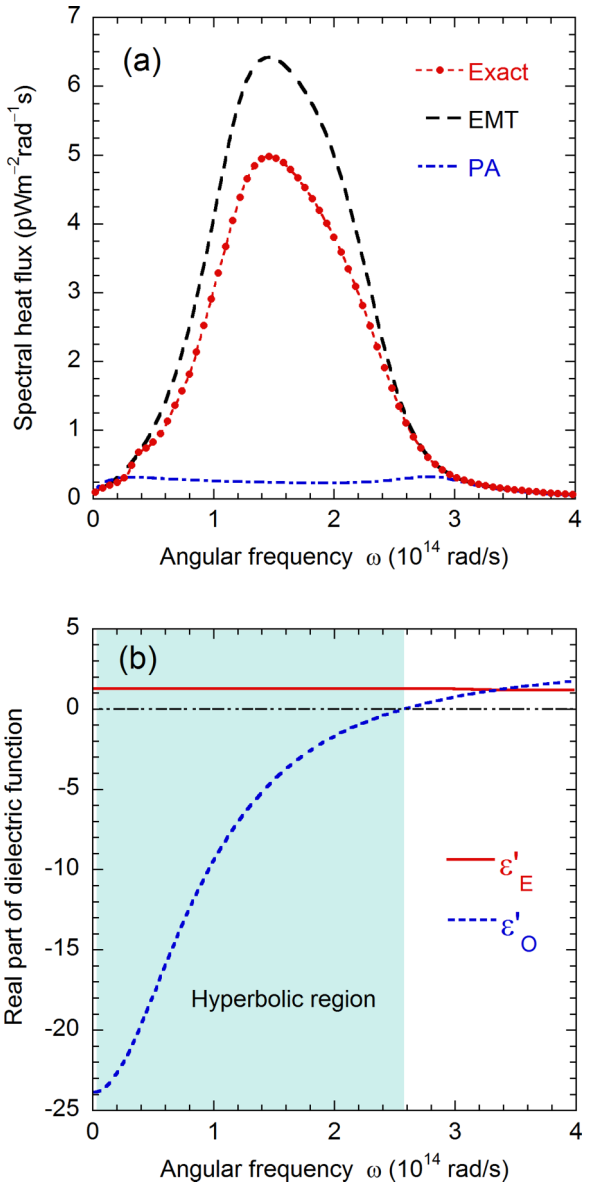

FIG. 4. (Color online) (a) Spectral radiative heat flux predicted by the scattering theory, EMT, and PA with the default parameters. (b) Effective dielectric functions for orthogonal directions for doped-silicon gratings with $f = 0.2$.

at large d, the major contribution comes from low-k modes with longer effective wavelengths. The EMT is valid when the effective wavelength is greater than the period. However, when the gap spacing exceeds 10 μm, beyond the characteristic wavelength of thermal radiation, photon tunneling effects become weak and the radiative heat flux will converge to the far-field values when the energy transfer is dominated by propagating modes and independent of the gap spacing.

With decreasing d, the exact solution deviates from the EMT result but approaches the PA prediction. Hence, the near-field radiative heat transfer tends to be localized at small gap spacing since the field will be highly confined due to the dominant contribution of high-k modes. Figure 3(b) also demonstrates that for the chosen values of f, H, and P, doped-silicon gratings outperform the bulk counterparts in terms of the heat-transfer enhancement for $d > 15$ nm. Another interesting phenomenon is that the near-field heat flux of doped-silicon grating exhibits a power law close to d^{-1} for submicron gap spacing rather than the well-known d^{-2} (obtained by assuming p-polarized waves have dominant contributions [56]) as is the case for both bulk and homogenized media supporting surface resonances.

C. Excitation of broadband hyperbolic modes

The underlying mechanism for the efficient radiative heat transfer is further explored by considering the spectral distribution, effective dielectric functions, and contour plot of the energy transmission coefficient. Using the default values, the exact solution gives a heat flux of 736 W/m^2, which is about eight times higher than the PA limit and 78% of the EMT limit. The heat-flux spectra predicted by the three methods are plotted in Fig. 4(a). It can be seen that the spectral heat flux

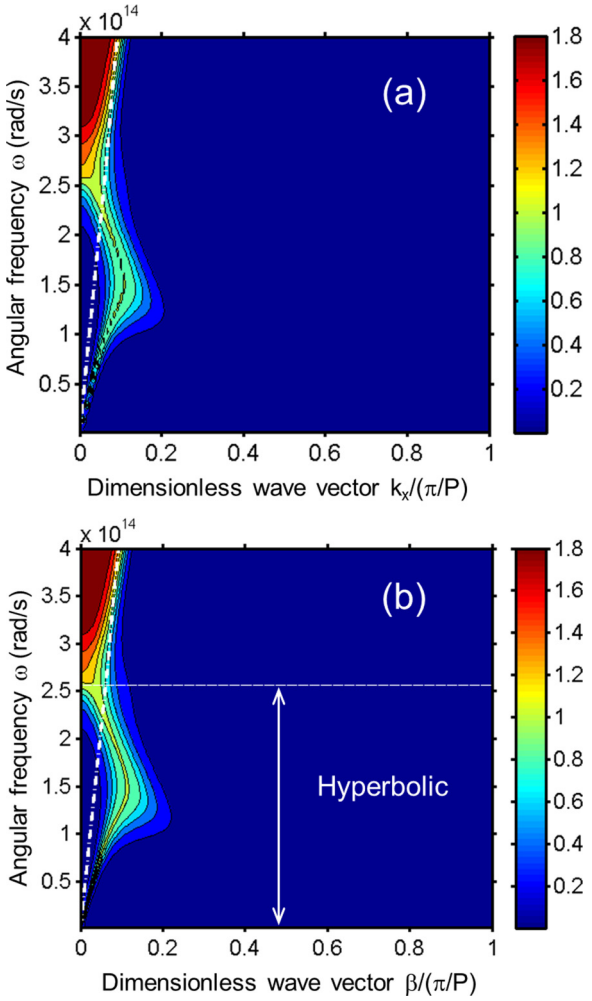

FIG. 5. (Color online) Contour plots of the energy transmission coefficient at $k_y = 0$ for the default parameters: (a) exact solution based on the scattering theory using the RCWA and (b) EMT by setting $\phi = 0$. The dash-dotted line denotes the light line.

predicted by the scattering theory is much higher than that by the PA from 3×10^{13} rad/s to 3×10^{14} rad/s. The surface resonance mode of doped Si lies at 2.88×10^{14} rad/s [31], where there is a small rise in the PA prediction. However, this feature does not show up according to the exact solution and EMT, both of which give a very similar trend in the spectral heat flux. The reason is further explored by considering the dielectric functions predicted by the EMT.

The real parts of the dielectric function in orthogonal directions ε'_O and ε'_E, calculated from Eqs. (6) and (7), are shown in Fig. 4(b). When ε'_O and ε'_E have different signs, the dispersion becomes hyperbolic with unbounded density of states [57,58]. As a result, high-k modes become propagating in the homogenized grating region. The local density of states becomes high, leading to broadband efficient photon tunneling [26]. The hyperbolic band ranges from very low frequencies to 2.58×10^{14} rad/s, as denoted by the shaded region in Fig. 4(b).

The energy transmission coefficient contour for $k_y = 0$ and $0 \leqslant k_x \leqslant \pi/P$ based on the scattering theory and EMT is given in Figs. 5(a) and 5(b), respectively. Because the cutoff wave vector for hyperbolic modes, defined as $1.94/d$ [35], is less than $2\pi/P$, only modes in the first Brillouin zone have nontrivial contributions to the radiative heat flux and the folding of other diffraction orders has negligible contributions. For the EMT, the calculation is set to $\phi = 0^\circ$ and $0 \leqslant \beta \leqslant \pi/P$, in which case the cross-polarization terms become zero. The energy transmission coefficient considers both s and p polarizations and hence the upper limit is 2 instead of 1 [31]. The agreement of the energy transmission coefficient predicted by both the scattering theory and the EMT is quite good. For s-polarized waves at frequencies below 2.58×10^{14} rad/s where $\varepsilon'_O < 0$, the gratings behave like a metal and give a very small ξ. At high frequencies, the energy transmission coefficient for s-polarized waves is large for propagating waves since ε'_O is greater than zero and ε''_O is small. However, photon tunneling for s-polarized waves contributes little to near-field radiation because of the negligibly small energy transmission coefficient (or tunneling probability). Attention is now paid to p-polarized waves as discussed next.

When $k_y = 0$, the reflection coefficient at the interface between vacuum and homogenized gratings for p-polarized waves is given as [31,59]

$$r_{\mathrm{pp}} = \frac{\sqrt{k_0^2 - k_x^2}\sqrt{k_0^2\varepsilon_E - k_x^2\varepsilon_E/\varepsilon_O} - \left(k_0^2 - k_x^2/\varepsilon_O\right)}{\sqrt{k_0^2 - k_x^2}\sqrt{k_0^2\varepsilon_E - k_x^2\varepsilon_E/\varepsilon_O} + \left(k_0^2 - k_x^2/\varepsilon_O\right)}. \quad (14)$$

Only r_{pp} is considered since neither s-polarized waves nor polarization coupling effects are important for high-k evanescent waves [31]. Considering that ε''_E (the imaginary part) is close to zero though not shown here, ε_E can be replaced by its real part ε'_E and Eq. (14) can be recast as follows:

$$r_{\mathrm{pp}} = \frac{\sqrt{\varepsilon'_E}\sqrt{k_0^2 - k_x^2} - \sqrt{k_0^2 - k_x^2/\varepsilon_O}}{\sqrt{\varepsilon'_E}\sqrt{k_0^2 - k_x^2} + \sqrt{k_0^2 - k_x^2/\varepsilon_O}}. \quad (15)$$

Note that for evanescent waves the imaginary part of r_{pp} must not be zero in order for the ξ to become nontrivial [31]. For the high-frequency region beyond the hyperbolic band, $\varepsilon'_O > 0$ and ε''_O is negligible; as a result, $\sqrt{k_0^2 - k_x^2/\varepsilon_O}$ becomes purely imaginary when k_x/k_0 is greater than $\sqrt{\varepsilon'_O}$, which is about 1 as shown in Fig. 4(b). The result is a very low tunneling probability at high frequencies. For propagating waves at high frequencies, ξ can still be large for p-polarized waves due to the dielectric behavior for both ordinary and extraordinary waves. Even though the combination of s- and p-polarized waves gives large ξ values $(1.0 - 1.8)$ in this region, the contribution from the high-frequency region to the total radiative heat flux is less than 10%.

In the hyperbolic region, $\varepsilon'_O > 0$ and ε''_O is large, so $\sqrt{k_0^2 - k_x^2/\varepsilon_O}$ has a dominant real part at low frequencies, leading to nontrivial energy transmission coefficients of evanescent waves. Doped-silicon gratings exhibit the unique property of hyperbolic modes with a large photon tunneling probability in a broad frequency band. This is the main reason for the enhancement of near-field radiation by gratings over bulk doped silicon. As shown in Fig. 5, even in the hyperbolic region, ξ is very small for low-k_x modes. When the hyperbolic film representing the grating region is thin, smaller than

the penetration depth of the slowly decaying low-k_x modes, the film becomes transparent. Due to the metallic feature of the doped-silicon substrate, the resulting ξ is very small in the hyperbolic band for low k_x values. This has been confirmed by calculations with increasing H, which results in higher energy transmission coefficient for low-k_x modes (although not shown here).

It is worth noting that thin-film effects also play a role such that the doped-silicon substrates act together with the hyperbolic film to enhance near-field heat flux for high-k_x modes. The demonstrated hyperbolic nature may come from the coupling with short-range SPPs [60]. The slight difference between Figs. 5(a) and 5(b) is that the hyperbolic band featured with a large energy transmission coefficient is slightly broader for an effective medium described by the EMT, suggesting that the hyperbolic dispersion at large wave vectors fails to hold for an actual doped-silicon grating. This explains why the EMT tends to predict a higher radiative heat flux than the exact solution. Similar phenomena have been noticed in multilayered metamaterials [35,58,61]. Overall, it can be clearly seen that the photon tunneling is effective in the hyperbolic region with a large number of k_x modes, except those very close to the light line. That is the reason why doped-silicon gratings support a much higher heat flux than bulk materials. Furthermore, since high-k_x modes become propagating in the gratings and the propagation length can exceed one period, near-field radiative transport with doped-silicon gratings tends to be delocalized; this explains why the PA fails as the period becomes sufficiently small.

D. Suppressed Casimir attraction

The formula for predicting the Casimir stiction between doped-Si gratings based on the scattering theory has been given in Eq. (13). The dielectric function of doped silicon at the imaginary frequency $\zeta = i\omega$ is given as [62]

$$\varepsilon(\zeta) = 1.035 + \frac{10.835\omega_0^2}{\omega^2 + \omega_0^2} + \frac{\omega_p^2}{\omega(\omega + \gamma)}. \tag{16}$$

Note that the first two terms on the right-hand side of Eq. (16) are the high-frequency dielectric response of silicon and are independent of the doping level. Here $\omega_0 = 6.6 \times 10^{15}$ rad/s is a fitted resonance frequency used to describe the interband transition for intrinsic silicon [62]. The last term of Eq. (16) represents the intraband contribution, where the values of ω_p and γ are given in Sec. II for a doping concentration of $10^{20}\,\mathrm{cm}^{-3}$. Note that the high-frequency dielectric response of silicon can be treated as a constant in the calculation of radiative heat transfer since the contribution from frequencies higher than 4.0×10^{14} rad/s is negligible. However, for the Casimir interaction, these high-frequency modes are significant and even dominant for gap distances below hundreds of nanometers. The Casimir force of doped-silicon gratings F_g normalized by that of bulk doped silicon F_b is plotted in Fig. 6 for varying submicron gap distances with two periods $P = 0.2$ and $1.0\,\mu$m for $f = 0.2$ and $H = 1\,\mu$m. The dashed lines with marks represent the results from the scattering theory using the RCWA. As shown as the dash-dotted line, the PA prediction is independent of the period and gap distance. Since the Casimir force is a strong function of

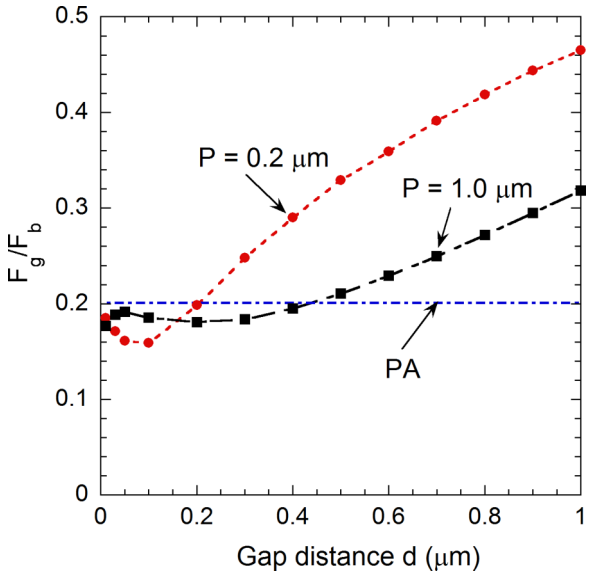

FIG. 6. (Color online) Casimir force between aligned doped-silicon gratings normalized to that for bulk counterparts as a function of the gap distances.

the distance between two parallel planar surfaces, the ratio F_g/F_b in the PA limit approaches the filling ratio of 0.2 for aligned gratings. In contrast to near-field energy transfer, the Casimir force is always reduced by surface corrugation as predicted by both the scattering theory and the PA method. Similar results were demonstrated for intrinsic silicon and metal gratings [54,63–65]. Nevertheless, the PA method may under- or overpredict the Casimir force as compared with the exact method. It is interesting to note that, according to the exact solution, the Casimir force of doped-silicon gratings is reduced to below the PA limit at gap distances below several hundred nanometers, which fall in the desired separation range for near-field energy harvesting and thermal management due to the prominently high radiative heat flux. The reason for the reduction of Casimir force below the PA limit may be attributed to the strong interactions of the fields between the ridges and those inside the grooves. Virtual photons confined between the ridges of the emitter and the receiver tend to leak when close to the edges. The Casimir force predicted by the scattering theory for $P = 1\,\mu$m tends to be closer to the PA limit than for $P = 0.2\,\mu$m. This is expected since both the edge effects and interactions between neighboring unit cells will become weak for increasing grating period. Therefore, besides improving the near-field radiative heat flux, patterning doped-silicon surfaces helps to relieve the Casimir stiction.

E. Effects of lateral displacement

The heat flux and Casimir force generally decrease when some lateral displacement δ is introduced between the top and bottom gratings since mode coupling is deteriorated due to symmetry breaking. Such an effect has been considered for potential devices such as thermal modulators [38]. Before possible applications of doped-silicon gratings in modulating the heat flux and attraction force, it is necessary to study the effects of lateral displacement. To simplify the analysis, the

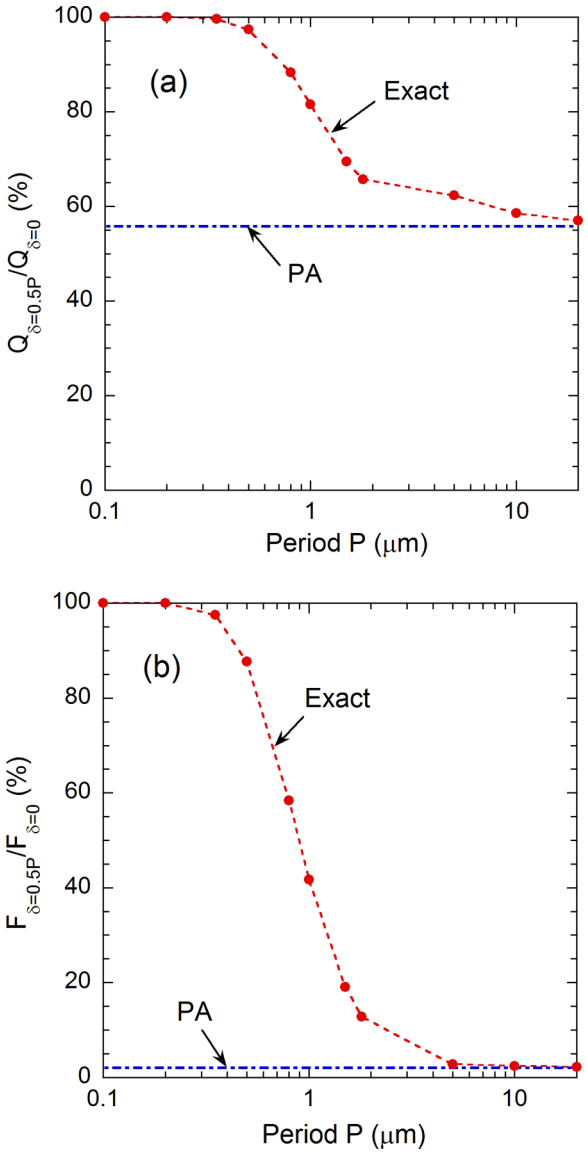

FIG. 7. (Color online) Ratio of (a) the radiative heat flux or (b) Casimir force for the misaligned grating when $\delta/P = 0.5$ to that corresponding to the aligned gratings as a function of the period.

relative lateral displacement δ/P is chosen to be 0.5, i.e., the maximum misalignment, so the heat flux and Casimir attraction force should be the smallest. The ratio of the radiative heat flux and Casimir force between the misaligned case and the aligned case, $Q_{\delta=0.5P}/Q_{\delta=0}$ and $F_{\delta=0.5P}/F_{\delta=0}$, are shown in Figs. 7(a) and 7(b), respectively, for varying grating period. When the period is small, below 200 nm, both the radiative heat flux and Casimir force remain the same, despite the misalignment. This is not surprising since when the period is shorter than the wavelength of the dominating modes, gratings behave as a homogeneous film according to the EMT. Even when $d = 0.5\,\mu$m, the heat flux and Casimir force for the misaligned case are still very close to that for the aligned case. Therefore, when the period is small, the heat flux and Casimir force for the doped-silicon gratings are insensitive to the displacement. As the period increases, there exists a strong dependence of both the radiative energy transfer and momentum transfer on the lateral displacement. As expected, if P exceeds 10 μm, both of the ratios approach those as governed by the PA limit. The PA limit of $Q_{\delta=0.5P}/Q_{\delta=0}$ is 56%, as seen from Fig. 7(a), while that of $F_{\delta=0.5P}/F_{\delta=0}$ is only 2%, as seen from Fig. 7(b). This is because the Casimir interaction is more sensitive to the gap spacing (d^{-4}) compared with the near-field radiative heat flux (d^{-2}).

IV. CONCLUSION

Highly efficient radiative heat flux between doped-silicon gratings is demonstrated and the amount can be as high as three times that between planar substrates. Furthermore, the exact solution based on the scattering theory predicts the heat flux to be 1–2 orders of magnitude higher than that given by the geometry-based approximation. The excitation of hyperbolic modes, which support broadband and large energy transmission coefficient for high-k modes, is attributed to be the main reason for the enhanced near-field energy transport. Meanwhile, the issue of Casimir stiction is demonstrated to be greatly relieved with gratings as compared to the bulk counterparts. This work offers possibilities of enhancing radiative energy transfer while simultaneously suppressing momentum exchange by patterning doped-silicon surfaces. The findings hold promise for applications in contactless thermal management, near-field energy harvesting, and relieving adhesion problems of MEMS devices.

ACKNOWLEDGMENTS

X.L. and Z.M.Z. were supported by the US Department of Energy, Office of Science, Basic Energy Sciences (Grant No. DE-FG02-06ER46343) and B.Z. was supported by the National Science Foundation (Grant No. CBET-1235975).

[1] Z. M. Zhang, *Nano/Microscale Heat Transfer* (McGraw-Hill, New York, 2007).
[2] S. Shen, Annu. Rev. Heat Transfer **16**, 327 (2013).
[3] A. I. Volokitin and B. N. J. Persson, Rev. Mod. Phys. **79**, 1291 (2007).
[4] K. Park and Z. Zhang, Front. Heat Mass Transfer **4**, 013001 (2013).
[5] Y. Xuan, Photon. Nanostr. Fundam. Appl. **12**, 93 (2014).
[6] K. Joulain, J. P. Mulet, F. Marquier, R. Carminati, and J. J. Greffet, Surf. Sci. Rep. **57**, 59 (2005).
[7] X. L. Liu, R. Z. Zhang, and Z. M. Zhang, ACS Photon. **1**, 785 (2014).
[8] M. Francoeur, R. Vaillon, and M. P. Mengüç, IEEE Trans. Energy Convers. **26**, 686 (2011).
[9] A. Narayanaswamy and G. Chen, Appl. Phys. Lett. **82**, 3544 (2003).

[10] R. S. DiMatteo, P. Greiff, S. L. Finberg, K. A. Young-Waithe, H. K. H. Choy, M. M. Masaki, and C. G. Fonstad, Appl. Phys. Lett. **79**, 1894 (2001).

[11] T. J. Bright, L. P. Wang, and Z. M. Zhang, J. Heat Transfer **136**, 062701 (2014).

[12] O. Ilic, M. Jablan, J. D. Joannopoulos, I. Celanovic, and M. Soljačić, Opt. Express **20**, A366 (2012).

[13] R. Messina and P. Ben-Abdallah, Sci. Rep. **3**, 1383 (2013).

[14] K. Park, S. Basu, W. P. King, and Z. M. Zhang, J. Quant. Spectrosc. Radiat. Transfer **109**, 305 (2008).

[15] Y. De Wilde, F. Formanek, R. Carminati, B. Gralak, P. A. Lemoine, K. Joulain, J. P. Mulet, Y. Chen, and J. J. Greffet, Nature (London) **444**, 740 (2006).

[16] A. C. Jones and M. B. Raschke, Nano Lett. **12**, 1475 (2012).

[17] C. R. Otey, W. T. Lau, and S. Fan, Phys. Rev. Lett. **104**, 154301 (2010).

[18] S.-A. Biehs, F. S. S. Rosa, and P. Ben-Abdallah, Appl. Phys. Lett. **98**, 243102 (2011).

[19] P. J. van Zwol, L. Ranno, and J. Chevrier, Phys. Rev. Lett. **108**, 234301 (2012).

[20] Y. Yang, S. Basu, and L. Wang, Appl. Phys. Lett. **103**, 163101 (2013).

[21] P. Ben-Abdallah and S.-A. Biehs, Phys. Rev. Lett. **112**, 044301 (2014).

[22] L. Cui, Y. Huang, J. Wang, and K.-Y. Zhu, Appl. Phys. Lett. **102**, 053106 (2013).

[23] J. G. Huang, Q. Li, Z. H. Zheng, and Y. M. Xuan, Int. J. Heat Mass Transfer **67**, 575 (2013).

[24] B. Guha, C. Otey, C. B. Poitras, S. Fan, and M. Lipson, Nano Lett. **12**, 4546 (2012).

[25] J. P. Mulet, K. Joulain, R. Carminati, and J. J. Greffet, Appl. Phys. Lett. **78**, 2931 (2001).

[26] S. A. Biehs, M. Tschikin, and P. Ben-Abdallah, Phys. Rev. Lett. **109**, 104301 (2012).

[27] B. Liu and S. Shen, Phys. Rev. B **87**, 115403 (2013).

[28] S. Basu and L. Wang, Appl. Phys. Lett. **102**, 053101 (2013).

[29] S. A. Biehs, P. Ben-Abdallah, F. S. S. Rosa, K. Joulain, and J. J. Greffet, Opt. Express **19**, A1088 (2011).

[30] B. Liu, J. Shi, K. Liew, and S. Shen, Opt. Commun. **314**, 57 (2014).

[31] X. L. Liu, R. Z. Zhang, and Z. M. Zhang, Int. J. Heat Mass Transfer **73**, 389 (2014).

[32] X. L. Liu, R. Z. Zhang, and Z. M. Zhang, Appl. Phys. Lett. **103**, 213102 (2013).

[33] I. S. Nefedov and C. R. Simovski, Phys. Rev. B **84**, 195459 (2011).

[34] A. Nemilentsau and S. V. Rotkin, Appl. Phys. Lett. **101**, 063115 (2012).

[35] X. L. Liu, T. J. Bright, and Z. M. Zhang, J. Heat Transfer **136**, 092703 (2014).

[36] B. V. Derjaguin, Kolloid Z. **69**, 155 (1934).

[37] K. Sasihithlu and A. Narayanaswamy, Phys. Rev. B **83**, 161406 (2011).

[38] J. Lussange, R. Guérout, F. S. S. Rosa, J. J. Greffet, A. Lambrecht, and S. Reynaud, Phys. Rev. B **86**, 085432 (2012).

[39] R. Guérout, J. Lussange, F. S. S. Rosa, J. P. Hugonin, D. A. R. Dalvit, J. J. Greffet, A. Lambrecht, and S. Reynaud, Phys. Rev. B **85**, 180301 (2012).

[40] X. L. Liu and Z. M. Zhang, Appl. Phys. Lett. **104**, 251911 (2014).

[41] G. Klimchitskaya, U. Mohideen, and V. Mostepanenko, Rev. Mod. Phys. **81**, 1827 (2009).

[42] A. W. Rodriguez, F. Capasso, and S. G. Johnson, Nat. Photon. **5**, 211 (2011).

[43] Y. Zheng and A. Narayanaswamy, Phys. Rev. A **83**, 042504 (2011).

[44] H. B. G. Casimir, Proc. K. Ned. Akad. Wet. **51**, 793 (1948).

[45] G. Bimonte and E. Santamato, Phys. Rev. A **76**, 013810 (2007).

[46] T. J. Bright, X. L. Liu, and Z. M. Zhang, Opt. Express **22**, A1112 (2014).

[47] Y. Bai, Y. Jiang, and L. Liu, J. Phys. D **47**, 445304 (2014).

[48] S. Basu, B. J. Lee, and Z. M. Zhang, J. Heat Transfer **132**, 023302 (2010).

[49] J. Shi, P. Li, B. Liu, and S. Shen, Appl. Phys. Lett. **102**, 183114 (2013).

[50] P. J. van Zwol, S. Thiele, C. Berger, W. A. de Heer, and J. Chevrier, Phys. Rev. Lett. **109**, 264301 (2012).

[51] E. Rousseau, M. Laroche, and J.-J. Greffet, J. Quant. Spectrosc. Radiat. Transfer **111**, 1005 (2010).

[52] X. L. Liu, L. P. Wang, and Z. M. Zhang, J. Heat Transfer **135**, 061602 (2013).

[53] R. Guérout, J. Lussange, H. B. Chan, A. Lambrecht, and S. Reynaud, Phys. Rev. A **87**, 052514 (2013).

[54] A. Lambrecht and V. N. Marachevsky, Phys. Rev. Lett. **101**, 160403 (2008).

[55] X. J. Wang, S. Basu, and Z. M. Zhang, J. Phys. D: Appl. Phys. **42**, 245403 (2009).

[56] J. J. Loomis and H. J. Maris, Phys. Rev. B **50**, 18517 (1994).

[57] Y. Guo, C. L. Cortes, S. Molesky, and Z. Jacob, Appl. Phys. Lett. **101**, 131106 (2012).

[58] C. L. Cortes, W. Newman, S. Molesky, and Z. Jacob, J. Opt. **14**, 063001 (2012).

[59] C. G. Malone, B. I. Choi, M. I. Flik, and E. G. Cravalho, J. Heat Transfer **115**, 1021 (1993).

[60] S. V. Zhukovsky, O. Kidwai, and J. E. Sipe, Opt. Express **21**, 14982 (2013).

[61] M. Tschikin, S. A. Biehs, R. Messina, and P. Ben-Abdallah, J. Opt. **15**, 105101 (2013).

[62] I. Pirozhenko and A. Lambrecht, Phys. Rev. A **77**, 013811 (2008).

[63] Y. Bao, R. Guérout, J. Lussange, A. Lambrecht, R. A. Cirelli, F. Klemens, W. M. Mansfield, C. S. Pai, and H. B. Chan, Phys. Rev. Lett. **105**, 250402 (2010).

[64] H. B. Chan, Y. Bao, J. Zou, R. A. Cirelli, F. Klemens, W. M. Mansfield, and C. S. Pai, Phys. Rev. Lett. **101**, 030401 (2008).

[65] F. Intravaia, S. Koev, I. W. Jung, A. A. Talin, P. S. Davids, R. S. Decca, V. A. Aksyuk, D. A. R. Dalvit, and D. López, Nat. Commun. **4**, 2515 (2013).